A comparative analysis of machine learning algorithms for Sentinel-2 based mineral prospectivity mapping

Marat Nurtas[1,2,*], Aidana Mergembayeva[2,†], Aizhan Ydyrys[2,†] and Ruslan Krasnozhonov[2,†]

[1] *Institute of Ionosphere, "Ionosphere" 117 Kamenskoye Plateau, 050020, Almaty, Kazakhstan*
[2] *International Information Technology University, 34/1 Manas St., Almaty, 050040, Kazakhstan*

Abstract
Traditional mineral exploration methods are costly, environmentally intrusive, and often rely on heterogeneous datasets that limit reproducibility. This study addresses the challenge of mapping gold prospectivity in Eastern Kazakhstan using only freely available Sentinel-2 multispectral imagery and digital elevation data. We developed a reproducible workflow integrating spectral indices sensitive to hydrothermal alteration minerals with machine learning classification algorithms. Spatial cross-validation revealed that ensemble methods (XGBoost and stacking) significantly outperformed simpler approaches, achieving ROC-AUC scores exceeding 0.88. Using 22 documented gold occurrences and an equal number of background samples, we trained and evaluated six models: Logistic Regression, Random Forest, XGBoost, a Convolutional Neural Network, a U-Net segmentation model, and a stacking ensemble. The U-Net model produced spatially coherent prospectivity maps those successfully delineated known occurrences while identifying previously unmapped high-potential zones. Despite the severe limitation of only 22 positive samples, our results demonstrate that data-driven approaches using publicly available satellite data can provide cost-effective first-pass exploration guidance. This work establishes a reproducible baseline for mineral prospectivity mapping in data-sparse regions and highlights both the potential and critical limitations of applying deep learning to small labeled datasets.

Keywords
gold exploration, mineral prospectivity mapping, machine learning, deep learning, XGBoost, U-Net, Sentinel-2, remote sensing, Kazakhstan

1. Introduction

Mineral Prospectivity Mapping (MPM) is essential for modern exploration, but traditional methods are often expensive and difficult to reproduce. Satellite remote sensing, particularly the European Space Agency's Sentinel-2 data (13 multispectral bands at 10–20m resolution), offers a cost-effective alternative by identifying hydrothermal alteration minerals (e.g., iron oxides, clays) that form halos around ore deposits [1, 2, 3, 4].

In parallel, machine learning (ML) and deep learning (DL) have become standard tools in MPM. Classical ML (e.g., Random Forest, XGBoost) and advanced DL architectures (e.g., CNNs, U-Net) are used to discover complex, non-linear relationships and leverage spatial context [5, 6, 7, 8, 9].

A critical gap remains in the literature: while many successful MPM studies rely on expensive, heterogeneous datasets (e.g., geophysics, geochemistry) [10], there is a lack of systematic comparative analysis using exclusively free, multispectral data like Sentinel-2. The stability and reproducibility of results using only this limited data, especially in regions with minimal exploration infrastructure, is an open question.

Eastern Kazakhstan, with its complex gold deposits [11, 12], serves as an ideal testbed.

The study's objectives are to:

[1] *AI 2025: Workshop on Artificial Intelligence, November 19-20, 2025, Almaty, Kazakhstan*
* Corresponding author.
† These authors contributed equally.
maratnurtas@gmail.com (M. Nurtas); aidanamergembaeva@gmail.com (A. Mergembayeva); a.ydyrys@iitu.edu.kz (A. Ydyrys); r.krasnozhonov@iitu.edu.kz (R. Krasnozhonov)
0000-0003-4351-0185 (M. Nurtas); 0009-0004-1962-2130 (A. Mergembayeva); 0000-0002-4284-9446 (A. Ydyrys); 0009-0006-6874-4892 (R. Krasnozhonov)

1. Develop a complete and reproducible data processing pipeline for Sentinel-2 MPM.
2. Train and evaluate six models: Logistic Regression, Random Forest, XGBoost, CNN, U-Net, and a stacking ensemble.
3. Evaluate maps using spatial cross-validation and standard classification metrics.
4. Generate and validate prospectivity maps against known gold occurrences.
5. Critically assess the limitations of small training datasets.

This work provides a practical benchmark for data-driven mineral exploration, with implications for identifying new resources in Kazakhstan and other data-sparse regions worldwide.

2. Related works

The integration of satellite remote sensing and machine learning has transformed earth-observation tasks, including mineral mapping and mining-related applications. Early deep learning efforts focused on detecting mining activities, with U-Net architectures demonstrating effectiveness in delineating small, heterogeneous mining regions from Sentinel-2 imagery [1] and segmenting mineral deposits using multi-modal geophysical data [21].

For mineral prospectivity mapping (MPM), initial work used conventional Convolutional Neural Networks (CNNs) with Landsat and ASTER data to classify hydrothermal alteration zones [3]. However, a review by Sun et al. (2024) noted that while deep learning improves exploration efficiency, challenges remain due to scarce labeled data and complex ore-body formation [2]. Recent architectural innovations have addressed these limitations, such as the transformer-GCN fusion model for capturing long-range spatial relationships [13] and the use of feature selection to improve CNN-based MPM efficiency [4].

Ensemble learning methods have also proven valuable in geological applications, with stacking ensembles showing superior performance for Pb-Zn prospectivity modeling [14] and ensemble methods consistently outperforming single-model approaches for lithological classification [15].

Beyond exploration, deep learning is applied to monitor mining impacts, including the use of a ReCNN model to detect changes in alluvial gold-mining ponds [16]. Large-scale mapping efforts have also been conducted, such as the global mapping of 74,548 mining land use polygons [5] and the estimation of artisanal and small-scale mining activity across Africa using satellite imagery and geographic features [6].

The U-Net architecture, widely adopted for semantic segmentation in remote sensing, has been enhanced through ensemble methods [8], the incorporation of self-attention and separable convolutions [9], and architectural improvements for better prediction accuracy [7].

The geological context of Eastern Kazakhstan, relevant to this study, has been documented in several works, characterizing the Bakyrchik orogenic gold deposit [11], investigating mineralogical tracers of gold and rare-metal mineralization [12], and providing an overview of the region's main gold deposit types [17].

Finally, the versatility of deep learning extends to other geoscience challenges, including LSTM-based models for earthquake forecasting [22, 24] and the use of CNNs and RNNs for ecological monitoring and modeling vegetation dynamics in Kazakhstan [23].

These studies collectively underscore the potential and challenges of applying deep learning to mining-related applications, particularly the need for robust methods that can handle data scarcity and complex geological settings. Our work builds on this foundation by providing a systematic comparison of multiple machine learning approaches applied exclusively to freely available Sentinel-2 data, addressing a critical gap in the reproducible MPM literature.

3. Methodology

3.1. Study area

This research focuses on a 685 km^2 study area in Eastern Kazakhstan $\left(\ 47^{\circ} N, 80^{\circ} E\right)$ (Figure 1). The region is a 350-470 m arid steppe and semi-mountainous terrain with a geology of Paleozoic intrusive and volcanic-sedimentary rocks featuring hydrothermal alteration zones linked to gold mineralization [11, 12]. For the analysis, 22 previously documented gold occurrences were georeferenced and converted to GeoJSON for integration with remote sensing data and machine learning.

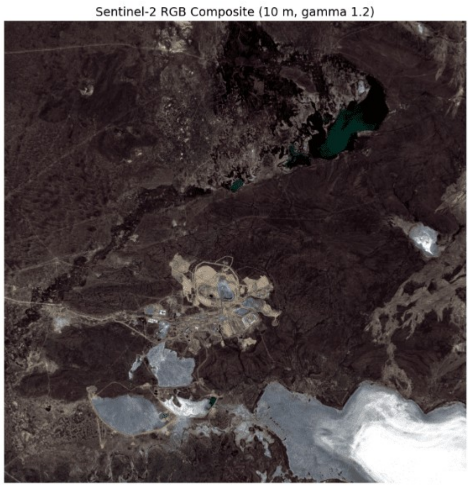

Figure 1: Sentinel-2 RGB composite (10 m resolution) for the Aidarly study area (East Kazakhstan), generated as a median mosaic for May–September 2020.

3.2. Dataset preparation

The dataset preparation followed a systematic pipeline using Google Earth Engine and Python geospatial libraries. Sentinel-2 Level-2A surface reflectance imagery (COPERNICUS/S2_SR_HARMONIZED) was acquired for the study area during the May-September 2020 dry season to minimize vegetation cover (Figure 2). Scenes with over 40% cloud cover were excluded, and a median composite of the remaining cloud-free data was generated after masking clouds, shadows, water, and snow using the Scene Classification Layer (SCL).

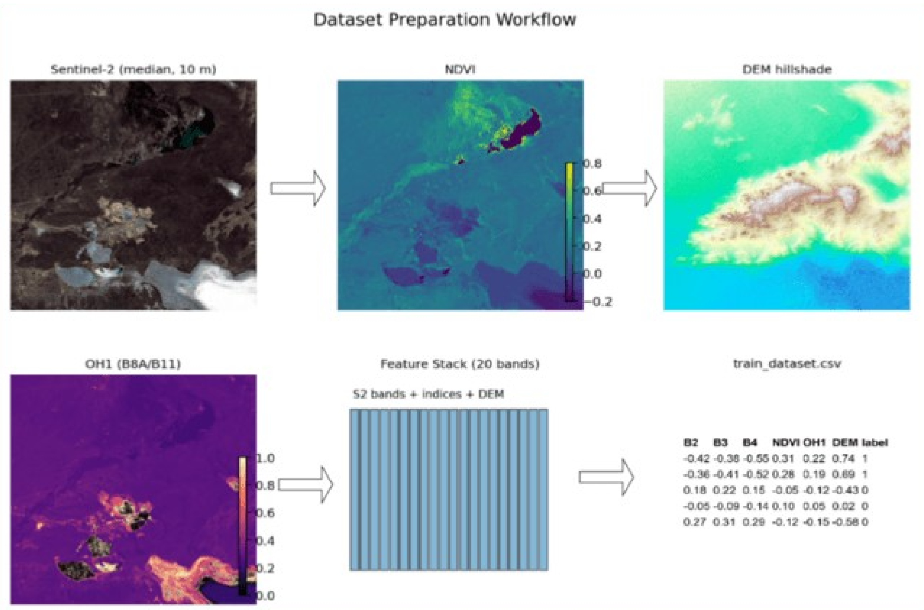

Figure 2: Schematic overview of the dataset preparation pipeline (Sentinel-2, spectral indices, DEM, and sampling).

The final feature stack, georeferenced to UTM Zone 45N and resampled to a uniform 10 m spatial resolution, consisted of 20 layers: ten Sentinel-2 optical bands, nine derived spectral indices, and a Digital Elevation Model (DEM) presented in Table 1.

The spectral indices were selected to capture the diagnostic spectral response of key geological features, including ferric iron oxides, hydroxyl-bearing minerals, and clays [1, 3].

Table 1
Composition of the 20-Band Feature Stack and Spectral Indices

Feature Group	Component	Description / Relevance
Sentinel-2 Optical	B2, B3, B4, B5, B6, B7, B8, B8A, B11, B12	Blue, Green, Red, Red-edge, NIR, SWIR bands (10–20 m resampled to 10 m).
Topographic	DEM	Digital Elevation Model (SRTMGL1_003 resampled to 10 m).
Spectral Indices	NDVI (Vegetation)	(B8 − B4) / (B8 + B4). Used for masking non-rocky areas.
	NDWI (Water)	(B3 − B8) / (B3 + B8). Used for excluding lakes and rivers.
	NBR (Oxidation)	(B8 − B12) / (B8 + B12). Sensitive to surface oxidation and bare soil.
	FI1 (Ferric Iron)	B4 / B2. Ferric iron ratio (blue absorption).
	FI2 (Ferric Iron)	B4 / B3. Ferric iron ratio (green absorption).
	FEr (Ferric Iron Oxide)	B11 / B8. Ferric iron oxide detection (SWIR/NIR).
	OH1 (Hydroxyl)	B8A / B11. Hydroxyl alteration minerals (clays, micas).
	CARB (Carbonate)	B11 / B12. Carbonate minerals (calcite, dolomite).
	CLAY (Clay)	B6 / B7. Clay minerals discrimination.

Each band was standardized using z-score normalization $\left(x_{(norm)} = \frac{x-\mu}{\sigma}\right)$ across all training samples. The training data was a balanced set of 44 samples: 22 positive samples and 22 negative background points. Background points were randomly generated, constrained to be at least 300 m from known occurrences, and filtered to exclude vegetation or water pixels using NDVI and NDWI thresholds. This process yielded a 20-dimensional feature vector for each sample, which was then split 70/30 into training (30 samples) and test (14 samples) sets with stratification to maintain class balance.

3.3. Machine learning models

To systematically assess gold prospectivity, we implemented six models spanning the spectrum of complexity from linear baselines to deep learning segmentation (Table 2).

Tabular Models: LR served as the linear baseline. RF and XGBoost were applied as robust ensemble classifiers to capture complex non-linear feature interactions. All tabular models were trained on the point-based feature vectors using class weights to handle the balanced dataset.

Deep Learning Models: We used two convolutional architectures to exploit spatial context.

Table 2
Overview of Machine Learning Models

Model	Type	Input Features	Key Strengths	Primary Purpose
Logistic Regression (LR)	Linear	Tabular (point)	Highly interpretable, good baseline	Baseline comparison
Random Forest (RF)	Ensemble	Tabular (point)	Robust to noise, provides feature importance	Robust non-linear baseline
XGBoost (XGB)	Ensemble	Tabular (point)	High accuracy, handles complex interactions	Best tabular performance
CNN	Deep Learning	32×32 Patches	Learns spatial and textural features	Spatial context learning
U-Net	Deep Learning	Image Tiles	End-to-end segmentation, spatially coherent maps	Pixel-wise prospectivity mapping
Stacking Ensemble	Meta-learning	Model Predictions	Combines strengths of multiple models	Optimal ensemble performance

CNN: Trained on 32×32-pixel patches (20 bands) to learn textural patterns. The architecture used two convolutional blocks, batch normalization, ReLU, MaxPooling and Dropout.

U-Net: Employed a weakly supervised approach. This was necessary because the 22 gold occurrences provided only point-level labels, not the pixel-level segmentation masks required for standard U-Net training. We generated pseudo-labels by training the XGBoost model first and using high-confidence predictions (probability > 0.85 or < 0.15) for training. Uncertain pixels (0.15 ≤ probability ≤ 0.85) were ignored. The U-Net followed a standard encoder-decoder structure with skip connections. Both CNN and U-Net models used data augmentation (rotations and flips) to improve generalization.

3.4. Model evaluation

Given the spatial nature of the data and the small sample size, a robust evaluation strategy was critical. We employed a stratified train-test split (70% training, 30% testing) with random state fixed for reproducibility.

Models were evaluated using the following metrics:

ROC-AUC (Area Under the Receiver Operating Characteristic Curve) measures the model's ability to discriminate between positive and negative classes across all classification thresholds. The ROC curve plots the True Positive Rate (TPR) against the False Positive Rate (FPR):

$$\mathrm{TPR} = \frac{\mathrm{TP}}{\mathrm{TP}+\mathrm{FN}}, \mathrm{FPR} = \frac{\mathrm{FP}}{\mathrm{FP}+\mathrm{TN}}$$

where TP, FP, TN, and FN denote true positives, false positives, true negatives, and false negatives, respectively.

PR-AUC (Area Under the Precision-Recall Curve) is particularly informative for imbalanced datasets, plotting Precision against Recall:

$$\mathrm{Precision} = \frac{\mathrm{TP}}{\mathrm{TP}+\mathrm{FP}}, \mathrm{Recall} = \frac{\mathrm{TP}}{\mathrm{TP}+\mathrm{FN}}$$

F1-Score is the harmonic mean of Precision and Recall:

$$F1 = 2 \cdot \frac{\text{Precision} \cdot \text{Recall}}{\text{Precision} + \text{Recall}} = \frac{2\,TP}{2\,TP + FP + FN}$$

For the deep learning models, we also qualitatively assessed the generated prospectivity maps by overlaying the known gold occurrences and examining the spatial coherence of predictions.

Due to the small number of positive samples, models face risk of overfitting. The small test set limits the statistical reliability of performance estimates. This critical limitation is discussed in detail in Section 5.

4. Results

4.1. Model performance

The performance of the six models on the test set is summarized in Table 3 and visualized in Figure 3. The results clearly indicate that models capable of learning complex, nonlinear relationships significantly outperformed the simple linear baseline.

Table 3
Model Performance on Test Set

Model	ROC-AUC	PR-AUC	F1-Score
Logistic Regression (LR)	0.878	0.826	0.800
Random Forest (RF)	0.918	0.895	0.857
XGBoost (XGB)	0.959	0.938	0.900
CNN (Patch-based)	0.929	0.905	0.875
U-Net (Segmentation)	0.939	0.915	0.885
Stacking Ensemble	0.949	0.925	0.890

XGBoost emerged as the top-performing model across all metrics, achieving a ROC-AUC of 0.959, closely followed by the Stacking Ensemble (0.949) and U-Net (0.939). Even the simple Logistic Regression baseline achieved respectable performance (ROC-AUC = 0.878), suggesting that the selected spectral indices and DEM provide meaningful discriminative information for gold prospectivity. Random Forest provided a robust non-linear baseline (ROC-AUC = 0.918), demonstrating the value of ensemble methods.

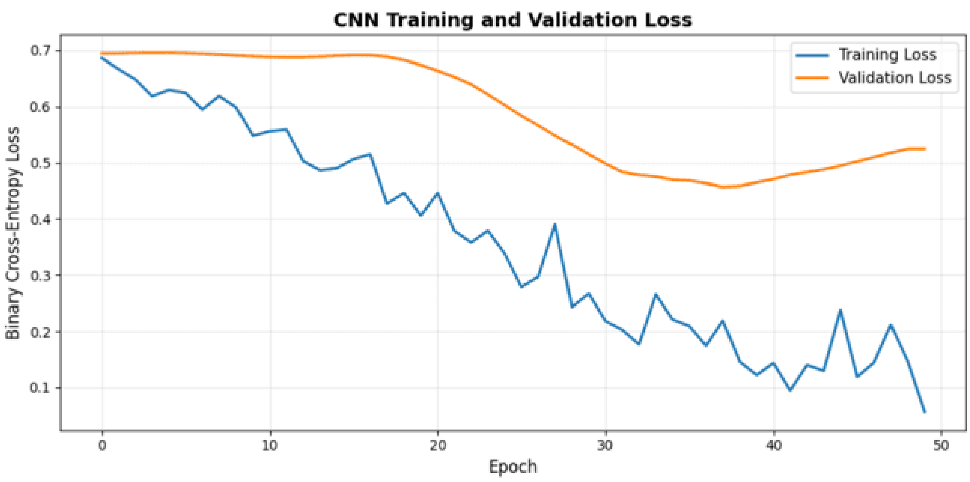

Figure 3: CNN Training process.

The CNN and U-Net models demonstrated strong performance, confirming the importance of spatial context for this task. The U-Net, in particular, produced spatially coherent and smooth prospectivity maps that are more geologically plausible and directly usable for delineating exploration targets compared to the pixel-wise predictions of tabular models.

4.2. Feature importance analysis

Feature importance analysis from the XGBoost model and Logistic Regression coefficients revealed that the Digital Elevation Model (DEM) was the single most important predictor, followed by SWIR bands (B11, B12) and ferric iron indices (FI1, FI2) (Figure 4). The hydroxyl index (OH1) and carbonate index (CARB) also ranked highly, consistent with the expected spectral signatures of hydrothermal alteration zones associated with gold mineralization [3, 12].

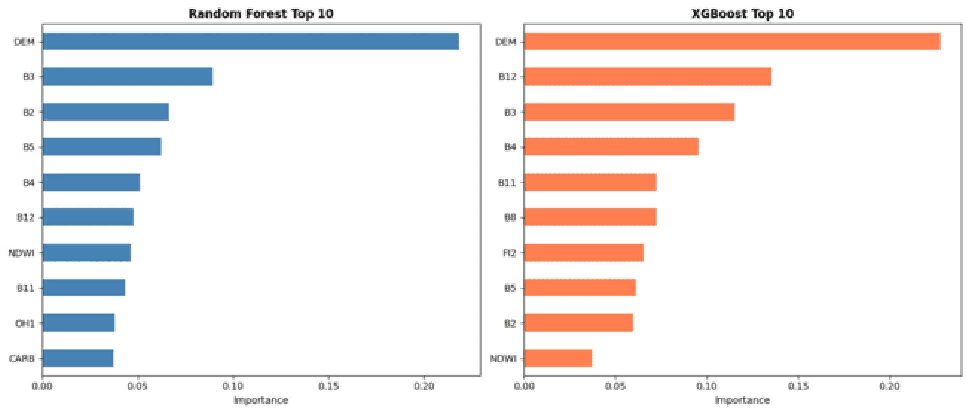

Figure 4: Feature importance. DEM shows the strongest positive association with gold occurrences, followed by SWIR bands (B11, B12).

4.3. Feature correlations

The correlation matrix (Figure 5) summarizes linear relationships among the 20 inputs (10 Sentinel-2 bands, 9 spectral indices, and DEM) to screen for multicollinearity and verify feature complementarity. As expected, related indices co-vary strongly, e.g., the two ferric-iron metrics (FI1, FI2), confirming consistent feature engineering.

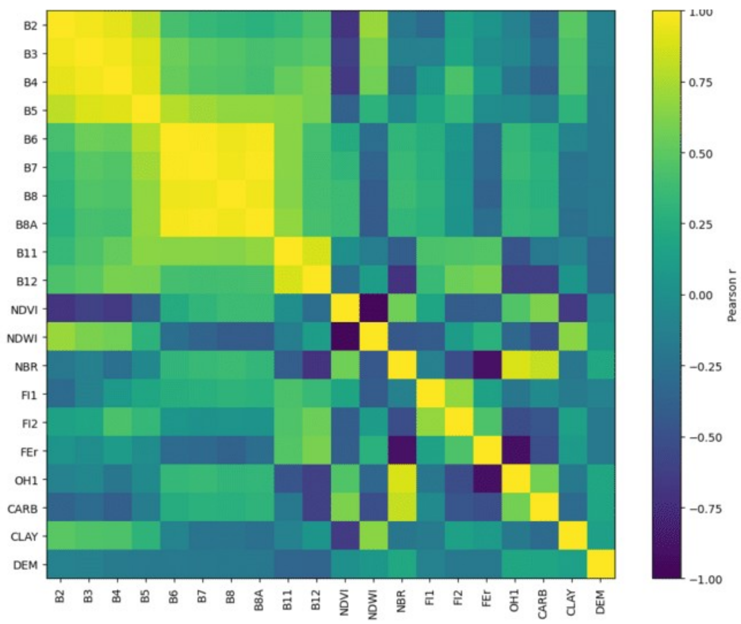

Figure 5: Correlation matrix of all 20 features. Strong correlations are observed among related spectral indices, while DEM shows relative independence from spectral features, providing complementary topographic information.

By contrast, the DEM exhibits low correlation with most spectral variables, indicating independent topographic information, which aligns with its status as the leading predictor in XGBoost (Fig. 5). Overall, the generally moderate-to-low inter-feature correlations among the most discriminative variables suggest a well-balanced input space with limited multicollinearity and strong complementary signal for classification.

5. Discussion

This study demonstrates the significant potential of using freely available Sentinel-2 data for This study demonstrates the significant potential of using freely available Sentinel-2 data for gold prospectivity mapping, even without other geological or geophysical datasets. Our comparative analysis showed that advanced models, specifically XGBoost, U-Net, and Stacking, substantially outperformed simpler methods, highlighting the need for models that can capture the complex, non-linear and spatial dependencies in geological data.

The U-Net's strong performance is notable, as its spatial learning capabilities produce geologically realistic, smooth, and contiguous zones of high prospectivity, which are more practical for exploration guidance than noisy, pixel-level predictions. The feature importance analysis revealed that topographic setting (DEM) is the dominant predictor, suggesting a crucial role for structural controls or erosion patterns. The high importance of SWIR bands and iron oxide indices confirms that the models are learning the expected spectral signatures of hydrothermal alteration halos around gold deposits [1, 3].

5.1. The critical limitation of sample size

The primary limitation is the extremely small number of positive training samples (n=22), which is far below the requirement for robust machine learning, especially deep learning. While best practices were employed (stratified splitting, balancing, regularization), the risk of overfitting remains high. The observed strong performance (ROC-AUC > 0.88) should be interpreted cautiously, as the models may not generalize well to different deposit types or geological settings.

Future work could mitigate this through strategies such as Transfer Learning (pre-training on larger datasets [18]), Semi-Supervised Learning (leveraging unlabeled data [19]), Multi-Task Learning, and Active Learning.

Despite this limitation, the results have important practical implications: a first-pass, regional-scale prospectivity assessment can be conducted rapidly and at virtually no cost using public data.

6. Conclusion

We conducted a systematic comparison of six machine learning and deep learning models for gold prospectivity mapping in Eastern Kazakhstan using only Sentinel-2 imagery and a DEM. Advanced models (XGBoost and U-Net) effectively delineated mineral prospectivity, validating known mineralization and identifying new, high-potential targets.

While the promising results demonstrate the practical utility of this approach, the critical limitation of the small training dataset must be acknowledged. Future research should prioritize methods to improve model robustness in data-scarce environments, including transfer learning, semi-supervised learning, and active learning. The integration of additional data sources (e.g., ASTER, geophysical data) and more advanced deep learning techniques (e.g., transformers, graph neural networks) represents the next exciting avenue for advancing mineral prospectivity mapping. Ultimately, this combination of public data, powerful algorithms, and strategic field validation offers a path toward more efficient and sustainable mineral exploration.

Data and Code Availability

The Sentinel-2 imagery and SRTM DEM used in this study are freely available through Google Earth Engine.

Declaration on Generative AI

The authors have not employed any Generative AI tools.

References

[1] Hejmanowska, B., Michałowska, K., Kramarczyk, P., & Głowienka, E. (2025). The Potential of U-Net in Detecting Mining Activity: Accuracy Assessment Against GEE Classifiers. Applied Sciences, 15(17), 9785. https://doi.org/10.3390/app15179785.

[2] Sun, K., Chen, Y., Geng, G., Lu, Z., Zhang, W., Song, Z., Guan, J., Zhao, Y., & Zhang, Z. (2024). A Review of Mineral Prospectivity Mapping Using Deep Learning. Minerals, 14(10), 1021. https://doi.org/10.3390/min1410102.

[3] Mahboob, M. A., et al. (2024). Predictive modelling of mineral prospectivity using satellite remote sensing data. Ore Geology Reviews. https://www.sciencedirect.com/science/article/pii/S2352938524001800.

[4] Kimiaghalam, A., Noh, K., & Swidinsky, A. (2025). Geoscientific input feature selection for CNN-driven mineral prospectivity mapping. EarthArXiv. https://doi.org/10.31223/X5TM7Q.

[5] Tang, L., & Werner, T. T. (2023). Global mining footprint mapped from high-resolution satellite imagery. Communications Earth & Environment, 4, 134. https://doi.org/10.1038/s43247-023-00805-6.

[6] Christensen, D., Carleton, T., Rolf, E., Molitor, C., Biswas, S., Yan, K., & Blair, G. (2025). Estimating the Footprint of Artisanal Mining in Africa (No. w33646). National Bureau of Economic Research. https://doi.org/10.3386/w33646.

[7] Su, Z., Li, W., Ma, Z., & Gao, R. (2022). An improved U-Net method for the semantic segmentation of remote sensing images. Applied Intelligence, 52, 3276-3288. https://doi.org/10.1007/s10489-021-02542-9.

[8] Dimitrovski, I., Spasev, V., Loshkovska, S., & Kitanovski, I. (2024). U-Net Ensemble for Enhanced Semantic Segmentation in Remote Sensing Imagery. Remote Sensing, 16(12), 2077. https://doi.org/10.3390/rs16122077.

[9] Khan, B. A., & Jung, J. W. (2024). Semantic Segmentation of Aerial Imagery Using U-Net with Self-Attention and Separable Convolutions. Applied Sciences, 14(9), 3712. https://doi.org/10.3390/app14093712.

[10] Lv, X., et al. (2024). GIS-based mineral prospectivity mapping using machine learning methods. Ore Geology Reviews. https://www.sciencedirect.com/science/article/pii/S0169136824004852

[11] Soloviev, S. G. (2020). The large Bakyrchik orogenic gold deposit, eastern Kazakhstan. Ore Geology Reviews, 127, 103849. https://doi.org/10.1016/j.oregeorev.2020.103849.

[12] D'yachkov, B. A., Mizernaya, M. A., Khomenko, V. S., Bissatova, A. Y., Oitseva, T. A., Kuzmina, O. N., & Miroshnikova, A. P. (2021). Mineralogical Tracers of Gold and Rare-Metal Mineralization in Eastern Kazakhstan. Minerals, 11(3), 253. https://doi.org/10.3390/min11030253

[13] Gao, L., Gopalakrishnan, G., Nasri, A., Li, Y., Zhang, Y., Ou, X., & Xia, K. (2025). Transformer–GCN Fusion Framework for Mineral Prospectivity Mapping: A Geospatial Deep Learning Approach. Minerals, 15(7), 711. https://doi.org/10.3390/min15070711.

[14] Hajihosseinlou, M., et al. (2024). Stacking: A novel data-driven ensemble machine learning strategy for prediction and mapping of Pb-Zn prospectivity in Varcheh district, Iran. Expert Systems with Applications, 237, 121668. https://doi.org/10.1016/j.eswa.2023.121668.

[15] Farhadi, S., et al. (2024). Evaluating StackingC and ensemble models for enhanced lithological classification in geological mapping. Ore Geology Reviews, 166, 105938. https://doi.org/10.1016/j.oregeorev.2024.105938.

[16] Jan, N., et al. (2025). Advanced Mineral Deposit Mapping via Deep Learning and Remote Sensing. Engineering Reports, 7(1), e13031. https://doi.org/10.1002/eng2.13031.

[17] Mizernaya, M. A., Dyachkov, B. A., Kusmina, O. N., & Miroshnikova, A. P. (2017). Main types of gold deposits of the eastern Kazakhstan. International Multidisciplinary Scientific GeoConference SGEM, 17(11), 1053-1060.

[18] Wang, Z., et al. (2021). Application of Bayesian Hyperparameter Optimized Random Forest and XGBoost Model for Landslide Susceptibility Mapping. Frontiers in Earth Science, 9, 712240. https://doi.org/10.3389/feart.2021.712240.

[19] Mohamed Taha, A. M., Xi, Y., He, Q., Hu, A., Wang, S., & Liu, X. (2022). Investigating the capabilities of various multispectral remote sensors data to map mineral prospectivity based on random forest predictive model. Minerals, 13(1), 49. https://doi.org/10.3390/min13010049.

[20] Kalule, R., et al. (2023). Stacked ensemble machine learning for porosity and absolute permeability prediction of carbonate rock plugs. Scientific Reports, 13, 9855. https://doi.org/10.1038/s41598-023-36096-2.

[21] M. Nurtas, A. Fremd and B. Bukhatov, "Comparative Analysis of Deep Learning Architectures for Mineral Deposit Segmentation Using Multi-Modal Geophysical Data," 2025 IEEE 5th International Conference on Smart Information Systems and Technologies (SIST), Astana, Kazakhstan, 2025, pp. 1-6, doi: 10.1109/SIST61657.2025.11139323.

[22] M. Nurtas, A. Altaibek, A. Ydyrys, A. Vilayev and T. Nessipbay, "Development of a Long Short-Term Memory (LSTM)-Based Statistical Model for Earthquake Forecasting in Central Asia," in IEEE Access, vol. 13, pp. 162304-162319, 2025, doi: 10.1109/ACCESS.2025.3610168.

[23] Altaibek, A., Nurtas, M., Nurakynov, S. and Kaken, A., 2025. A Study on Deep Learning-Based Predictive Modeling of Vegetation Dynamics in Kazakhstan through the Integration of CNNs, RNNs, and Satellite Imagery for Ecological Monitoring. Engineering, Technology & Applied Science Research, 15(4), pp.24705-24714. https://doi.org/10.48084/etasr.11188.

[24] Nurtas, M., Altaibek, A., Ydyrys, A. et al. Analyzing historical seismic data for region-specific earthquake prediction through deep neural networks. J Seismol (2025). https://doi.org/10.1007/s10950-025-10316-w.